3-1-2024

Lateral load response of semi-interlocking mortarless masonry-infilled frames

Sonam Dorji

Hossein Derakhshan

David P. Thambiratnam

Alireza Mohyeddin
Edith Cowan University
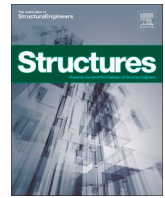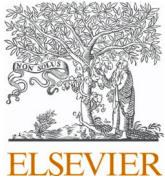
Lateral load response of semi-interlocking mortarless masonry-infilled frames

Sonam Dorji [a], Hossein Derakhshan [a,*], David P. Thambiratnam [a], Alireza Mohyeddin [b]

[a] *Faculty of Engineering, Queensland University of Technology, Brisbane, QLD 4000, Australia*
[b] *School of Engineering, Edith Cowan University, Joondalup, WA 6027, Australia*

ARTICLE INFO

ABSTRACT

Structural frames infilled with masonry material called masonry-infilled frames (MIFs) are common types of constructions around the world. These structures generally have mortared masonry as infill material which made the buildings stiff during past earthquakes and generated additional torsional forces. With a view to improve the seismic performance of MIFs this paper presents the results of a numerical simulation study on the behaviour of previously-tested MIFs with semi-interlocking masonry (SIM) material. In a simplified micro-modelling approach, the concrete and masonry materials are simulated using Concrete Damaged Plasticity technique and the joints are considered as zero-thickness cohesive interfaces modelled using traction-separation model. The numerical model is then used to study the lateral load response of the alternate MIF with SIM. The methodology for FE modelling of MIFs with SIM as an infill material is developed and explained in detail. The numerical models incorporate the sliding of the masonry units under the application of lateral loads. It is shown that the models capture the experimental results quite well although the modelling technique has certain limitations. The outcomes of a sensitivity analysis on the effects of the interface mechanical properties are presented along with discussion of limitations and suggestions for future improvements.

1. Introduction

Masonry-infilled frames (MIFs) are common types of constructions around the world [1–8] but the presence of mortared masonry infill in buildings has been associated with catastrophic earthquake damages [9–16]. Some of the earthquake damage has been linked to increased stiffness of frames due to the presence of masonry infill [17] which have the potential to create torsional forces within the building according to the distribution in plan. Alternative infill materials or construction methods have been researched increasingly in the past decade.

Internationally, the existing literature includes both experimental and numerical studies of infilled frames with sliding [18–25] or plastic joints [26]. Some research has focused on out-of-plane response characteristics [e.g. 18] whilst others primarily investigated the in-plane response. Semi-interlocking masonry (SIM) originated in Australia has been experimentally investigated in a few studies including Hossain et al. [27,28] and Dorji et al. [29]. In Hossain et al. [28], the SIM-infilled frames were found to have relatively high energy dissipation capacity which was attributed to shear sliding between the masonry units. The high energy dissipation capacity is a structural property that is

advantageous during earthquake loading. The newer study [29] observed that SIM-infilled frames have smaller initial stiffness in comparison to traditional MIFs which can potentially reduce the torsional forces. The study [29] also found that sliding occurred between masonry courses which resulted in repairable damage at relatively low drift ratios. This behaviour at low drifts seemed to prevent other forms of damage including the commonly observed shear cracking of reinforced-concrete elements in traditional MIFs [30–33] which is attributed to the formation of diagonal struts in the masonry infills [33–35]. Notwithstanding, the infill damage increased with drift such that at extreme drifts (e,g, over 5%; see Fig. 1) almost all vertical mortar joint (infill-column interface) had spalled and sliding between joints was quite visible and irreparable. While these drift ratios should not be practically encountered in buildings, the condition in Fig. 1 is presented solely to illustrate the significance of masonry joint in-plane sliding.

To create a computer model and validate it, a literature review was conducted. The sliding phenomenon described above and shown in Fig. 1 is generally absent in the damage patterns reported for traditional MIFs, and hence some of the macro- and micro-modelling [36] techniques developed for the structures are unsuitable for SIM-infilled frames.

Nomenclature

δ_n^0, δ_s^0 and δ_t^0 Separation of joints at the damage initiation in Mode I, Mode II and Mode II directions respectively

δ_n^f, δ_s^f and δ_t^f Separation of joints at complete failure in Mode I, Mode II and Mode II directions respectively

f_c, f_m, f_{mg} and f_{cg} Average compressive strengths of concrete, ungrouted and grouted masonry prisms, and grout cylinder respectively

f_{ct}, f_{mt}, f_{tg} and $f_{ct.f}$ Average tensile strengths of concrete, ungrouted masonry prism, grouted masonry prism and grout cylinder respectively

h Height of MIF from the top of foundation to centre of beam

K_{nn}, K_{ss} and K_{tt} Elastic stiffness coefficients of interface in Mode I, Mode II and Model III respectively

t_n^0, t_s^0 and t_t^0 Limiting traction strengths of interface in Mode I, Mode II and Model III respectively
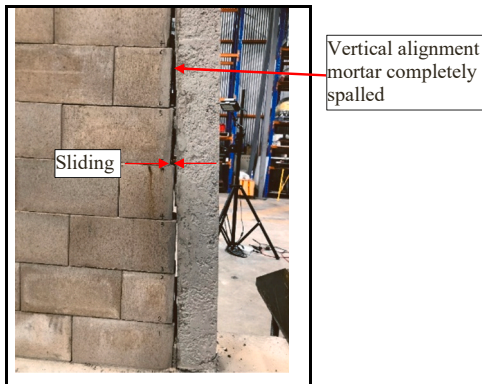
l Length of MIF between column centres

Fig. 1. Relative sliding of the masonry courses [19].

This research was therefore developed with a first objective of incorporating the sliding phenomenon in numerical models. Furthermore, a feature of SIM construction is that it requires to be core-filled with grout to meet insulation requirements against fire, moisture, etc. The presence of grout presents a curious case as it restricts the sliding between joints. However, low-strength grout can induce controlled sliding in joints given the inherent bed-joint weakness in the in-plane direction. This was observed in the experimental campaign [29], in which one specimen that had a low-strength grout underwent limited joint sliding. Its stiffness was still significantly smaller than traditional masonry infills [29]. Therefore, the second objective of the current study was to investigate grout effect numerically using the validated computer model.

While the current study presents an overview of the salient characteristics of this construction type, both modelling and related experimental study limitations have been highlighted throughout the paper. Future refined studies would be required to confirm the suitability of this kind of infill for construction, including aspects such as dynamic response, out-of-plane stability (despite interlocking features), local dislodgment of blocks due to sliding, and refined studies on grout effects. These research areas that can inform resilient earthquake designs are further highlighted throughout the paper including in the Conclusions.

This paper includes a brief overview of the relevant literature on modelling discontinuous surfaces using interface elements within Abaqus [37], followed by a brief description of the recently completed SIM-infilled frame tests [29] that were used for numerical modelling. A FE modelling strategy for in-plane loaded SIM-infilled frames is then explained and used to reproduce the results of one bare frame and four MIFs. Finally, detailed discussions on the FE results and sensitivity analyses are presented.

1.1. Review of numerical modelling

In general, infilled frames have been modelled using macro-modelling, meso-modelling, micro-simplified, or micro-detailed approaches, with an overview of the modelling strategies being discussed by [19]. Macro-modelling assumes the whole masonry infill as only a few structural elements such as panel, beam, struct, etc [38,39] requiring minimal number of elements. In micro-simplified modelling, concrete and masonry materials are often considered as continuum solid elements and modelled using Concrete Damaged Plasticity (CDP) model [36,40,41] whilst the mortar joint may be simplified as an interface. The masonry materials are typically constructed as solid 3D deformable parts using C3D8R elements [42]. According to [43], determination of all material model parameters would require large experimental testing, and therefore, the properties that cannot be tested within the typically limited budget of studies are selected from the literature. This approach was also taken in the current study as discussed later. Micro-detailed approaches would include modelling of mortar joints as well as masonry material [19] and are quite extensive to run.

In the micro-simplified method used herein, the frame-masonry infill interfaces, the bed-joints and the perpends were specified as interfaces. the interfaces were assumed as zero-thickness cohesive elements modelled using traction-separation behaviour discussed below. The length and the height of the masonry units were increased on either side by half the perpend and bed joint thicknesses respectively as was the case also in several earlier studies [36,44,45].

The traction-separation was assumed as a bilinear relationship (see Fig. 2) that requires the elastic stiffness coefficients and the damage initiation criterion characterisation. The stiffness coefficients are K_{nn}, K_{ss} and K_{tt} in Mode I (normal), Mode II (in-plane shear) and Mode III (out-of-plane shear) directions respectively that the users must specify. 'Quadratic nominal stress' [37] is commonly used to specify the damage initiation of the interface by using the limiting strengths (t_n^0, t_s^0, t_t^0; see Fig. 2). After the interface has failed, the contact of the materials is generally modelled as 'Hard-contact' in the normal direction and friction in the tangential directions [44,46]. The 'Hard-contact' model prevents the surrounding materials to penetrate each other [36,38].

A review of the micro-simplified (interface) modelling in traditional MIFs was conducted in this study to gain confidence in modelling MIFs with SIM infill. The studies have generally adopted the same frame-masonry infill interface properties for both the bed joints and the perpends in the masonry infill as shown in Table 1. It can be seen from Table 1 that the mechanical properties can vary significantly (from 0 to 74.4 MPa/mm for stiffness coefficients and from 0.00001 to 0.311 for
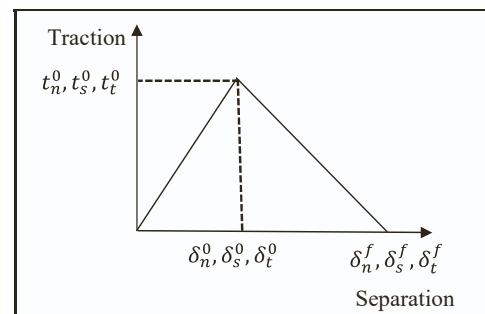

Fig. 2. Bilinear relationship of cohesive material. Re-drawn from [43].

Table 1

Interface properties from past studies for traditional MIFs.

Parameters	Frame-masonry infill			Bed joints and perpends		
	Kareem et al. [36]	Khatiwada & Jiang [47]	Emami et al. [50]	Kareem et al. [36]	Khatiwada & Jiang [47]	Emami et al. [50]
K_{nn} (MPa/mm)	0	17.9	11	0	17.9	11
K_{ss} (MPa/mm)	36.6	74.4	11	36.6	74.4	11
K_{tt} (MPa/mm)	36.6	NR	11	36.6	NR	11
t_n^0 (MPa)	0.00001	0.311	0.1	0.00001	0.311	0.15
t_s^0 (MPa)	0.17	0.311	0.15	0.17	0.311	0.20
t_t^0 (MPa)	0.17	NR	0.15	0.17	NR	0.20

NR: Not reported

limiting strengths) which can be attributed to the different scopes of the research in the respective studies. For example, the masonry infill in Kareem et al. [36] was made of clay bricks while in Khatiwada & Jiang [47] concrete masonry units were used. Since the present study deals with mortarless masonry, the interface properties for this construction type were also reviewed that showed high variability (see Table 2) due to different masonry materials used in the investigations. The materials included SIM in Zahra [48] and masonry units with shear keys in Shi et al. [49]. In addition, the former study tested mortarless masonry made of concrete units while in the latter study the masonry was constructed using clay bricks. No documented studies could be found that investigated mortarless masonry as an infill material using the traction-separation model in Abaqus [37].

2. Experimental programme

Versaloc SIM units produced by Adbri Masonry [51] were used in the original experimental study [29], and the masonry units are shown in Fig. 3. The masonry units included end- and standard-units, with both unit types having dimensions of 400 (length) × 200 (height) × 150 mm (thickness) with 32.2 mm thick face-shell. The half-unit had the length halved to 200 mm while the other dimensions were same with that of the other two unit types. The lugs located on top and the tongue and grooves (T&G) that interlock the units at the sides (see Fig. 3c) prohibit the relative out-of-plane movements of the units. Similarly, the lugs and T&Gs eliminate the need for bed-joint and head-joint mortars. The lack of mortar facilitates in-plane movements between the masonry units that are restrained only by friction. The five MIFs that are subjects of this study are listed in Table 3 and Fig. 4 [29].

As detailed in Table 3, one bare frame and four MIFs (see Fig. 4) were tested in the experimental study [29]. Specimen 2 was similar to the bare frame except that it was infilled with SIM, ungrouted and without vertical load. Specimen 3 was narrower (length-wise) than Specimen 2 by one masonry unit length (400 mm) hence having an aspect ratio of 1.22 compared to 0.95 for Specimen 2. Specimen 4 was almost identical to Specimen 2 except that it was subjected to a vertical load of 40 kN on each column and a uniformly distributed load of 6.17 kN/m (or 10 kN total) on beam. This loading arrangement approximately represented that applied on the ground floor of a two-storeyed building. Finally, Specimen 5 was similar to Specimen 2 but a low-strength grout was used to fill the masonry unit cores. All specimens were subjected to cyclic displacements imposed at the left end of the beam. Detailed material

Table 2

Interface properties for mortarless masonry prisms subjected to compression.

Parameters	Zahra [48]	Shi et al. [49]
K_{nn} (MPa/mm)	28	2.18×10^4
K_{ss} (MPa/mm)	32	0
K_{tt} (MPa/mm)	32	NR
t_n^0 (MPa)	0.68	0.68
t_s^0 (MPa)	0.82	0
t_t^0 (MPa)	0.82	NR

NR: Not reported

properties of the Versaloc units are reported in [52], of which a summary is included in Tables 4 and 5. That study [52] found that only a part of the face-shell thickness (19 mm, see Fig. 3c) participated in taking the compressive load and that width was used to calculate the strengths of masonry prisms. Another major observation of the material testing was that the tensile strength of the grouted wallet was equal to the grout tensile stress as indicated in Table 5.

3. FE modelling

The bare frame was first created and calibrated against the experimental results, and the verified model was used to develop a numerical model of Specimen 2, which entailed the calibration of masonry-related parameters including various interface properties. The geometries, vertical load conditions or masonry properties of the verified model of Specimen 2 was next modified to check for calibration against the experimental data for Specimens 3 to 5 without changing the interface properties. A detailed explanation of the procedure is given in the following sections.

3.1. Specimen 1 (bare frame)

The frame members were constructed as solid 3D deformable parts using C3D8R elements. A partition surface of 150 × 130 mm that corresponded to beam cross-section was created at the inner face of the columns at top to enable rigid beam-column connection using 'tie' constraint available within Abaqus [37]. The same dimension partition surface was made at the outside face of the columns to apply lateral displacement which is discussed later. Next, the longitudinal and transverse reinforcing bars were constructed as 2-node 3-dimensional (T3D2) elements and placed in their respective positions using 'embedded region' available in Abaqus [37], and it allows for the perfect bond development between concrete and rebars [53,54]. A clear cover of 20 mm was provided from the outside of concrete to the edge of the transverse bars to replicate the original construction details.

Concrete material was simulated using CDP with the modulus of elasticity (20,213.8 MPa) being obtained from material testing. Poisson's ratio of 0.2 was adopted from [55]. Similarly, a dilation angle (ψ) of 40 degrees was assumed based on the suggestion of [53] and recognising that [56] found that the commonly used value for concrete masonry ranges from 30 to 45 degrees. A viscosity value (μ) of 0.01 was chosen in this study instead of the Abaqus [37] default value (zero) in order to enhance the solution convergence [57,58]. To improve the convergence of numerical integrations in the relatively long displacement range appropriate for the tested SIM-infilled frames, a large viscosity was used in this study instead of the values commonly used (0.001) for analysis of traditional MIFs in the small displacement range [36,55]. It is highlighted that the sensitivity analyses of the plasticity parameters have been extensively conducted in the past studies [53,56, 58–60] that found that the response of traditional MIFs are highly dependent on them. Other plasticity parameters include eccentricity (ϵ), f_{b0}/f_{c0} ratio and shape factor, K_c which were maintained as per the suggested default values in the Abaqus [37] software (respectively 0.1,
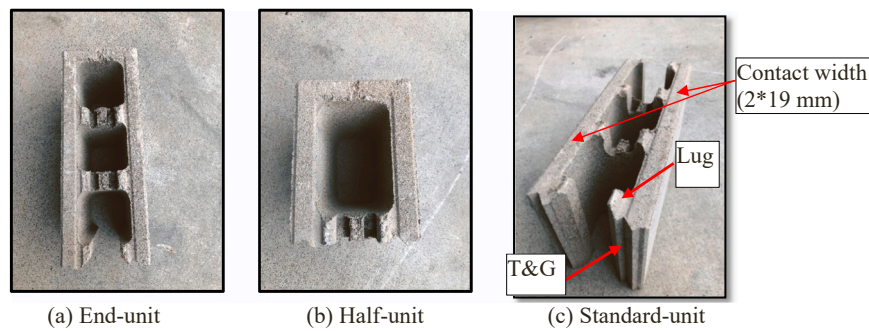
Fig. 3. Types of 150 mm series Versaloc concrete masonry units.

Table 3
Specimens tested in [29].

ID	h (mm)	l (mm)	Aspect ratio, h/l	Vertical load	Grout
Specimen 1	1675	1770	Bare frame		
Specimen 2	1675	1770	0.95	No	No
Specimen 3	1675	1370	1.22	No	No
Specimen 4	1675	1770	0.95	Yes	No
Specimen 5	1675	1770	0.95	No	Yes

1.16, and 0.67).

The inelastic compressive behaviour given in Fig. 6(a) was obtained from experimental testing with the initial yield approximated at 60% of the maximum strength following [48]. There was hardly any softening branch on the tensile stress-strain relationship of the cylinders that were tested using Brazilian splitting test [61]. Therefore, except for the failure stress that was obtained from testing (2.38 MPa; see Table 5), a parabolic tensile behaviour shown in Fig. 6(b) was assumed which is similar to the approximations adopted in [5,36,41]. The reinforcing bars had a yield stress of 500 MPa which were modelled as elastic-perfectly plastic similar to that in [62]. The modulus of elasticity of 200,000 MPa [53,63] and Poisson's ratio of 0.3 [36,53,63] were assumed from the literature.

3.2. Specimen 2

To construct a numerical model of Specimen 2, the calibrated bare frame was infilled with SIM using a micro-modelling approach. Masonry material was simulated using CDP with the modulus of elasticity from experiment and Poisson's ratio from literature (see Table 6) forming the elastic part. The parabolic relationships in Fig. 7 for compression and tension were developed, respectively, by assuming initial yield at 60% and failure stress at 100% of maximum strengths. While the maximum strength in compression was obtained from material testing, premature sliding of the top course was observed in the tensile testing of the ungrouted wallets (see Table 5) and therefore a suitable tensile strength of ungrouted wallets from the frictional component was considered which is explained below. A much higher compressive ultimate strain was required in the ungrouted wallets in comparison to that of the concrete and grouted wallets due to the flexible behaviour of the ungrouted wallets which was as a result of the presence of a dry joint in between the masonry units [52].

In the design of MIFs, additional horizontal and vertical 'alignment mortar' (see Fig. 5) was provided between the frames and the infill [29]. The horizontal mortar included 5 mm thick mortar between the beam and the masonry infill, and another 5 mm mortar between the foundation and the masonry infill. The vertical alignment mortar was provided between the column and the masonry infill which were 10 mm thick on both sides of the masonry infill. It is highlighted that Fig. 1 shows that this vertical layers completely spalled by the time the drift ratio reached in excess of 5%.

The horizontal alignment mortar thickness (10 mm) was divided

equally among the number of masonry courses (8) which resulted in the masonry units height of 201.25 mm instead of the actual height (200 mm). A similar procedure was performed to distribute the vertical alignment mortar thickness (20 mm) to the length of the masonry units. In the courses with the end- and standard-units, the units were extended to 405 mm from 400 mm. In the courses that had the half- and standard-units, the standard-units were maintained with the same 405 mm length elsewhere which led to the half-units being longer than actual size by 2.5 mm (extended length of 202.5 mm). In relation to the thickness of the masonry, the masonry was simplified as solid with a 38 mm thickness for all masonry unit types based on the contact width shown in Fig. 3. Other methods of considering masonry include that of hollow units as done in [41].

The above method of distribution resulted in the dimensions (length × height × thickness) of 405 × 201.25 × 38 mm for the end- and standard-units, and 202.5 × 201.25 × 38 mm for the half-units. Similar to concrete, the masonry was constructed as solid 3D deformable parts using C3D8R elements and then interconnected with Interface elements as shown in Figs. 8 and 9. Meshing size was 32 × 32 mm which was similar to 30 × 30 mm and 35 × 35 mm suggested in [53] and [56] respectively, and the mesh size resulted in four and five elements across the beam and column depths respectively.

The horizontal and vertical interfaces were modelled using different interface elements recognising the damage patterns that were observed in these surfaces. Cracking to vertical alignment mortar was the first damage that occurred in the MIF specimens during experiment [29], and these mortar joints completely spalled by the end of the tests (see Fig. 1). In contrast, the horizontal alignment mortar suffered much lesser damage compared to the vertical alignment mortar. In the masonry infill, the bed joints underwent sliding, while the perpends were mostly found to be intact. In view of these observations, the column-masonry infill and the bed joint interfaces were simulated using traction-separation cohesive model (see Fig. 9), while the beam-masonry infill interface and the perpends were modelled as rigid joints using 'tie' [37]. This method of 'tie' was also introduced in connecting the frame members to masonry infill in traditional MIF studies in [64] and [65]. It is highlighted that introducing a tie at head-joints presents a significant limitation on the model, making it unsuitable for modelling flexural-dominated infilled frames. In such structures (infills with high axial ratio), perpend joints could slide vertically. Therefore, the numerical model is considered to be appropriate only for the infill with similar aspect ratios. The horizontal sliding that occurred in the global X direction shown in Fig. 9 corresponded to Mode I (K_{nn}) and Mode II (K_{ss}) deformations for the column-masonry infill and the bed joint interfaces respectively.

In assigning material model properties for the vertical interfaces (column-masonry infill interface), t_{n0} was assumed as 0.20 MPa due to unavailability of test data (see Table 7). This value is the default masonry bond strength recommended in the Australian masonry standard AS 3700 [66]. In addition, based on AS 3700 recommendations on masonry material properties, a constraint was applied between the shear
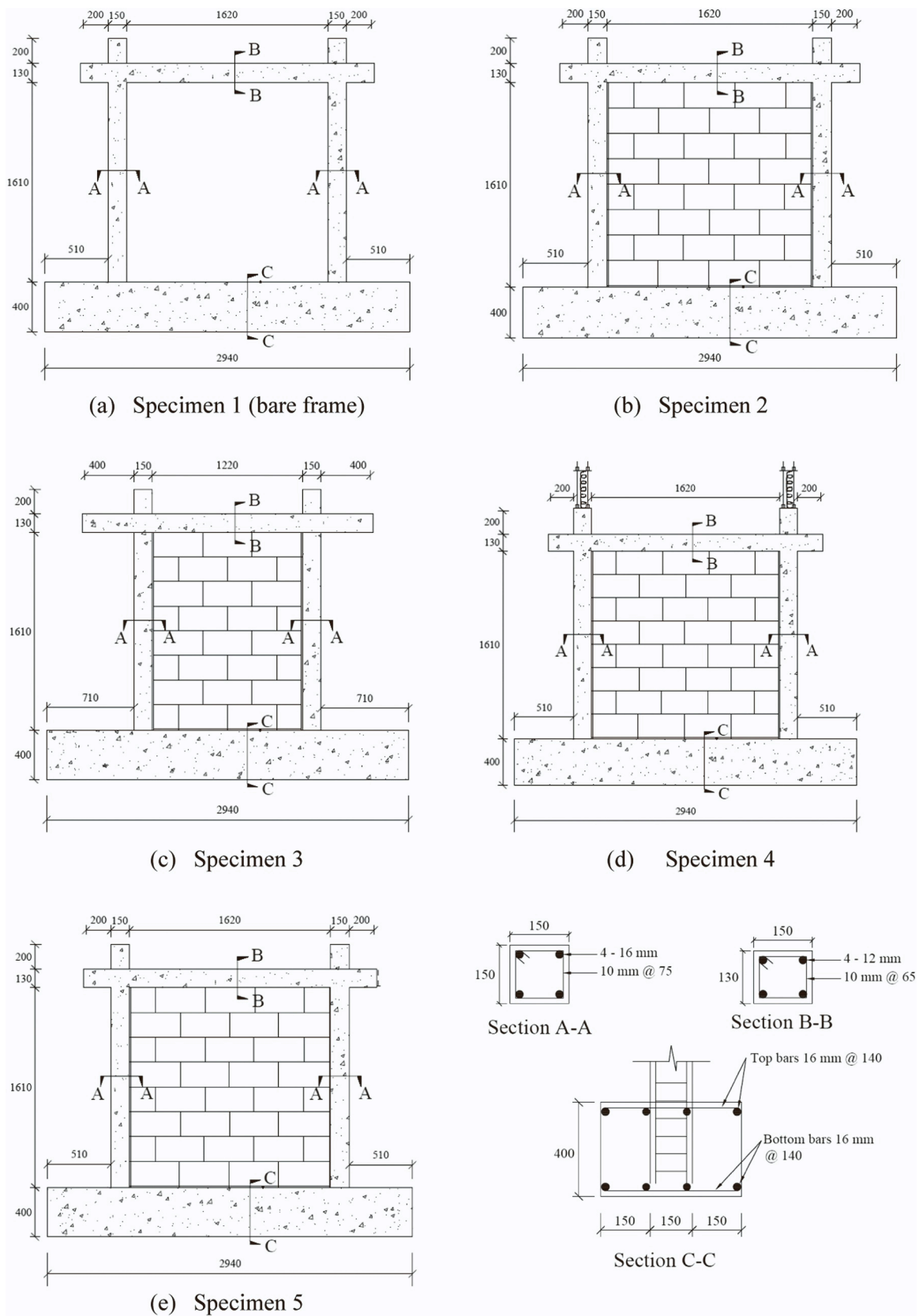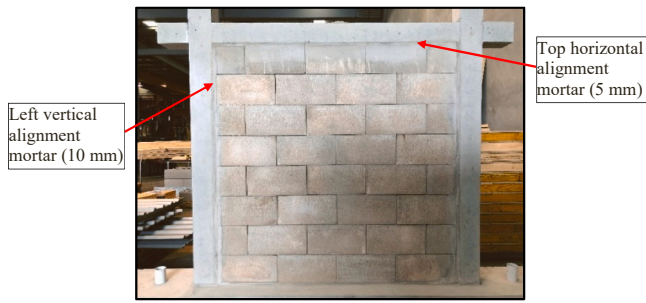
Fig. 4. Specimen details [29].

Fig. 5. Typical MIF specimen.

Table 4
Compressive strength.

Material	No. of Samples	Mean (COV)
Concrete, f_c, (MPa)	10	20.51 (17.8%)
Ungrouted prism, f_m, (MPa)	4	20.68 (17.2%)
Grouted prism, f_{mg}, (MPa)	4	12.21 (5.6%)
Grout, f_{cg}, (MPa)	3	6.23 (19.4%)

Table 5
Tensile strength.

Material	No. of Samples	Mean (COV)
Concrete, f_{ct}, (MPa)	10	2.38 (10.7%)
Ungrouted wallet, f_{mt}, (MPa)	4	Premature sliding
Grouted wallet, f_{tg}, (MPa)	3	0.53 (19.9%)
Grout, $f_{ct,f}$, (MPa)	3	0.53 (3.7%)

strength and normal (bond) strength at these interfaces such that t_{s0} and t_{t0} were equal to 1.25 times t_{n0}.

For bed joints properties, t_{n0} which is the tensile strength of ungrouted wallet was assumed as the product of axial stress at the mid height of the masonry infill and the coefficient of friction as proposed in [52] for mortarless masonry constructions. The frictional coefficient for SIM has been suggested in [28] as 0.75. Assuming this coefficient and an axial stress of 0.036 MPa, t_{n0} was estimated as (i.e. $0.036 \times 0.75 =$)

0.027 MPa. While t_{s0} of the bed joint was approximated to be 1.25 times t_{n0} following the AS 3700 [66] guideline, t_{t0} was provided with a relatively high value (1 MPa) to represent the lugs and T&G connections that prohibited the out-of-plane movement of the masonry units as discussed in the Experimental Programme section. 'Quadratic nominal stress' [37] was used to initiate damage in the cohesive interfaces which when failed was modelled by 'hard-contact' [44] in the normal behaviour. In the tangential directions, a frictional coefficient of 0.75 was assigned according to recommendation by [28]. Table 7 shows the stiffness coefficients that produced the best match of the experimental curve in the calibration process which is discussed later.

3.3. Specimen 3

The masonry infill width of the verified model of Specimen 2 was decreased to check for calibration against the experimental data of Specimens 3. This new width included the vertical alignment mortar thickness of 20 mm, which was distributed among masonry units in a similar manner that was discussed for Specimen 2. Since there were three units in the courses that contained end- and standard-units, the mortar thickness was increased to the nearest multiple of 3 which was 21 mm. The resulting masonry unit dimensions were $407 \times 201.25 \times 38$ mm for end- and standard-units, and $203.5 \times 201.25 \times 38$ mm for half-units.

During the testing it was found that one half-block at the end of infill was dislodged out-of-plane by 5 mm at 0.6% drift but the dislodgment did not progress. This out-of-plane movements (see [29] for full details) was considered isolated and hence not reflected in the numerical modelling. However, unlike in other specimens, there were imperfections due to casting with minor construction defects in Specimen 3 frames (see Fig. 10). These imperfections were presumed to be the reason why the initial modelling of Specimen 3 using the reference specimen properties produced stronger and stiffer behaviour than experimental measurements. Kalkan [67] reported that a reduced modulus of elasticity, E, in the analytical model was adequate to replicate the experimental results of reinforced concrete beams with geometrical imperfections. In the present study, the imperfections were considered by reducing the flexural stiffness EI where I is the frame moment of inertia. It was found that if the overall concrete-related (e.g. frame) stiffness in Specimen 3 is reduced by approximately 50%, a good

(a) Compressive properties

(b) Tensile properties
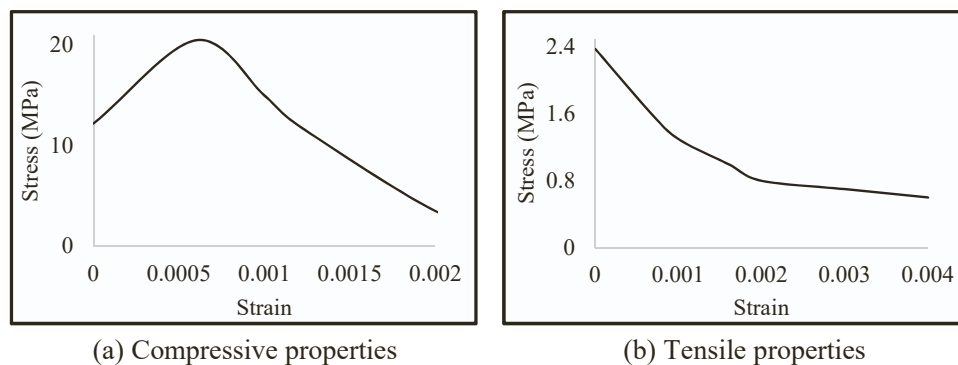
Fig. 6. Stress-inelastic strain relationship of concrete.

Table 6
CDP properties for infilled masonry.

Material	Elasticity		Plasticity				
	Modulus of elasticity (MPa)	Poisson's ratio	Dilation angle	Eccentricity	f_{b0}/f_{c0}	K	Viscosity
Concrete (as per the bare frame)	20,213.80	0.2	40	0.1	1.16	0.67	0.01
Ungrouted prism	6558.16						
Grouted prism	7842.25						

(a) Compressive properties (ungrouted)

(b) Tensile properties (ungrouted)

(c) Compressive properties (grouted)

(d) Tensile properties (grouted)
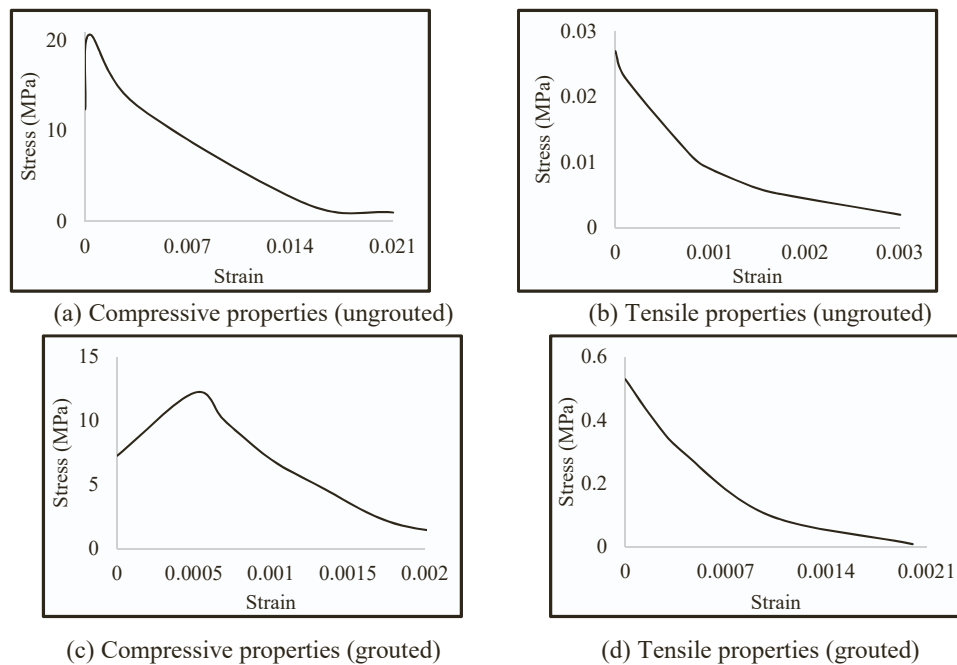
Fig. 7. Stress-cracking strain relationship of masonry.
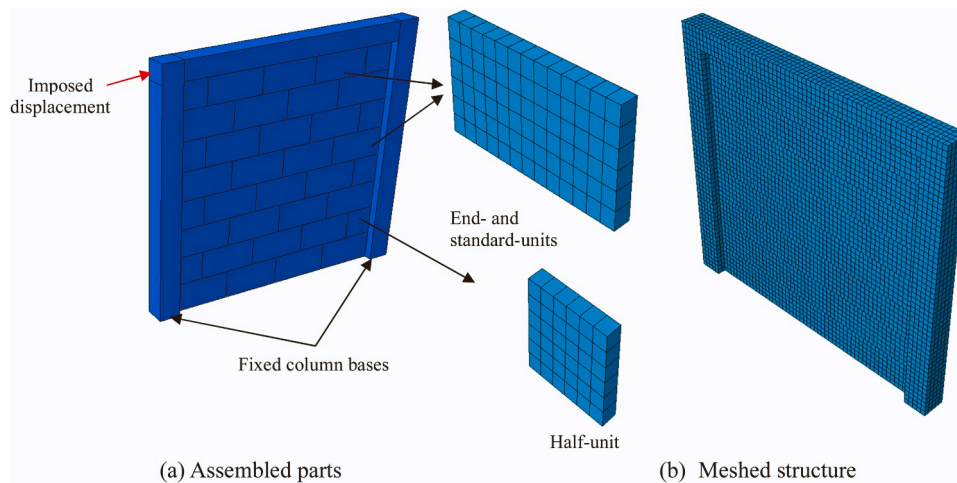

(a) Assembled parts

(b) Meshed structure

Fig. 8. 3D view of the model.

balance between the calculated initial stiffness and peak strength and the experimental counterparts are obtained. For the purpose of stiffness adjustment, the frame cross-section dimensions were decreased from 150 × 150 mm to 130 × 130 mm for the columns and 150 × 130 mm to 130 × 110 mm for the beam. In addition, a reduced *E* value of 18, 000 MPa was assumed. The combination of new *EI* corresponded to the reduction in elastic *EI* of 51% and 47% respectively for the columns and the beam.

3.4. Specimen 4

The frame members of the validated Specimen 2 model were applied with vertical loads for calibration against the experimental data of Specimen 4. These vertical loads were 40 kN on each column and 10 kN on the beam. The loads were converted as pressure loads which corresponded to 1.78 MPa and 0.04 MPa applied at the top of the columns and the beam respectively. These vertical loads were applied before the lateral displacement was being imposed on the structure.

3.5. Specimen 5

As discussed in [29], sliding of masonry units in Specimen 5 was widespread due to which the same ungrouted specimen's interface definitions of traction-separation model in the column-masonry infill and bed joint, and "tie" [37] in beam-masonry infill and perpends were used. The masonry material and bed joint interface properties of the validated Specimen 2 model were changed, with the new values being listed in Table 8. This change was necessary to incorporate the grouting effect for calibration against the experimental results of Specimen 5, which are explained below.

Except for the modulus of elasticity which was obtained from the experiment, Poisson's ratio and the plasticity parameters of Specimen 5 were considered to be same as those for the ungrouted masonry (see Table 6). Similarly, the parabolic inelasticity behaviour given in Figs. 6 and 7 were developed by assuming initial yield at 60% and failure stress at 100% of their respective maximum strengths which were both obtained from the material testing.
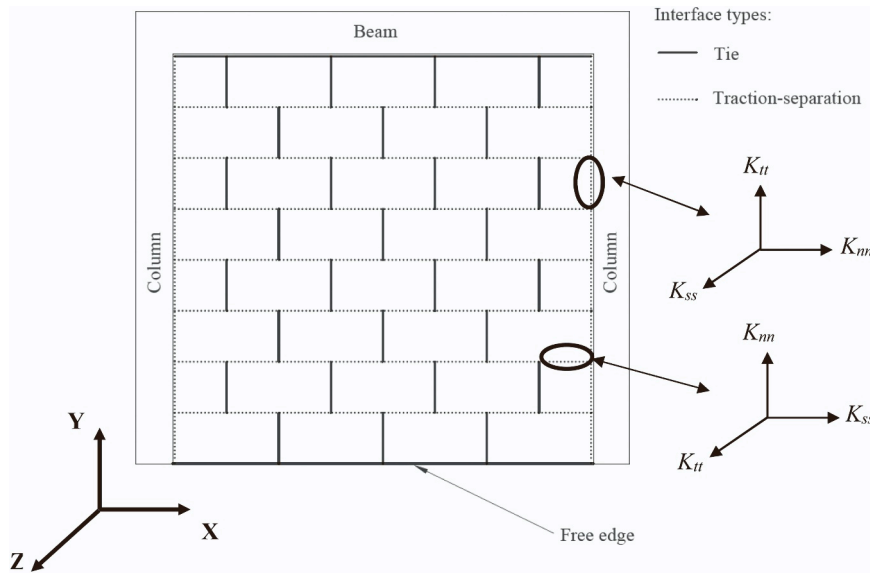
Fig. 9. Interface surfaces.

Table 7
Interface properties for Specimens 2, 3 and 4.

Interface	Stiffness (MPa/mm)			Limiting strength (MPa)		
	K_{nn}	K_{ss}	K_{tt}	t_{n0}	t_{s0}	t_{t0}
Column-Masonry infill	0.15	1	0.04	0.20	0.25	0.25
Beam-Masonry infill	Tie					
Bed joint	0.85	0.11	10	0.027	0.034	1
Perpend	Tie					

Table 8
Interface properties for Specimen 5.

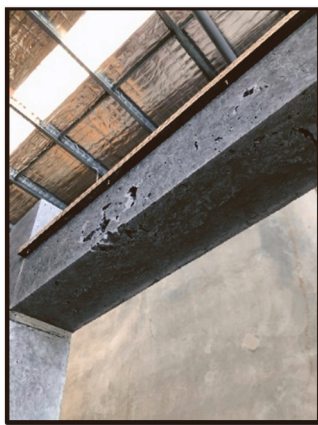| Interface	Stiffness (MPa/mm)			Limiting strength (MPa)		
	K_{nn}	K_{ss}	K_{tt}	t_{n0}	t_{s0}	t_{t0}
Column-Masonry infill	0.15	1	0.04	0.25	0.25	0.25
Beam-Masonry infill	Tie					
Bed joint	1.0	0.85	10	0.53	0.66	5
Perpend	Tie					

Fig. 10. Minor construction defects in Specimen 3 frame.

For bed joints, t_{n0} of 0.53 MPa was obtained from the tensile testing of grouted wallets (see Table 5). Similar to ungrouted specimens, t_{s0} was made equal to 1.25 times t_{n0}, and a significantly high value of t_{t0} due to the presence of interlocking mechanisms and grouts was assumed in Specimen 5. The column-masonry infill interface properties were unchanged from that of the ungrouted specimens due to the vertical alignment mortar being used in both ungrouted and grouted specimens in the experiment. Additionally, 'Quadratic nominal stress' [37] was used for interfaces damage initiation, and the interfaces were modelled as 'hard-contact' [44] in the normal behaviour and a frictional coefficient of 0.75 in the other directions was assigned at failure (Table 8).

3.6. Displacement-controlled analysis

The validation was performed for push direction as recommended in ASCE 41–17 [6]. The initial boundary condition of the specimens included fixing the column base (Fig. 8) to represent the relatively stiff concrete foundation used in the experiment. The lateral displacement was applied through a 'Ramp' option [37] which allows the displacement to be monotonically increased until the maximum displacement is reached. This maximum displacement was specified corresponding to the maximum test displacement of the respective specimens. In applying the boundary conditions and the lateral displacements, a reference point was created at the centre of the column bases and beam cross-section at the left end (see Fig. 8) and connected rigidly over the whole surface. At each analysis step, the displacement was recorded along with the sum of forces at the base of the columns in the negative direction to the imposed displacement. The force-displacement relationship of the specimens was constructed using the recorded displacement and force. In doing the analysis, a high specification computer with a 32 GB RAM and 11th generation Intel i7 with 3.0 GHz processor was used.

4. Results and discussion

Fig. 11 presents the comparison of cracking pattern in the experimental investigation to that of the stresses obtained from FE modelling. The FE models adequately capture the crack formation in the experimental investigations. In addition, it is observed that the damage in the frame members of the MIFs is similar to that of the bare frame. This finding implies that the presence of SIM infill did not critically alter the damage patterns of MIFs in comparison to the bare frame which is advantageous from the seismic loading point of view.

A comparison of the force-displacement behaviour of specimens obtained from the FE modelling against the experimental results is
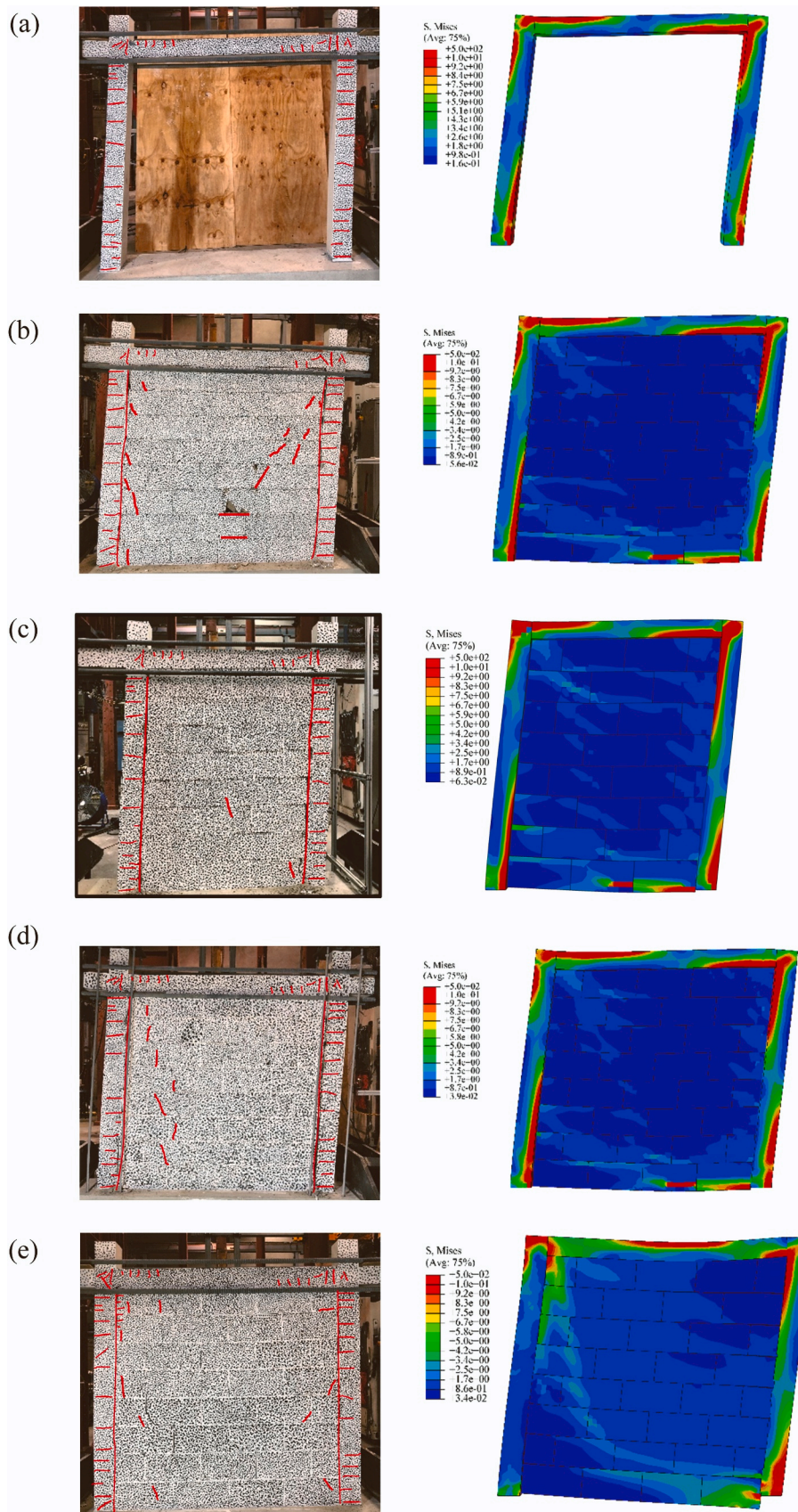
Fig. 11. Crack patterns in experimental and FE modelling of (a) Specimen 1 (b) Specimen 2 (c) Specimen 3 (d) Specimen 4 (e) Specimen 5.

shown in Fig. 12. For convenience, the figure scales have been kept the same across Specimens 1 to 4, which had comparable ranges of behaviour. It can be seen from Fig. 12 that the overall calculated behaviour matched reasonably well with the experimental force-displacement relationship, however there are some discrepancies as discussed below.

A distinctive, almost linear, initial stiffness can be found for most specimens including for the bare frame and most notably for Specimen 3. This behaviour is replaced by a curved response in the FE modelling, which in most cases overestimates the experimental stiffness. Furthermore, the post-peak response of Specimen 5 is notably different from the calculated behaviour. Both of these differences are attributed in part to the difference in the loading scenario; the cyclic nature of the experimental loading means the actual response includes strength and stiffness degradation whilst the capacity calculations using commercial software under monotonic loading does not accommodate these degradations. This difference is well-documented in the related literature, e.g. [see 68–70]. It is highlighted that for even for the bare frame, the initial stiffness and the peak strength could not be simultaneously achieved with good accuracy reflecting the strong cyclic loading effects. The overestimation of the frame stiffness in Specimen 1 propagated into similar trends for the rest of the specimens. It is recommended that in future numerical models capable of reproducing cyclic response be used for analysis.

The overestimation of the peak strength in Specimen 4 at a significantly large drift of 4% is attributed to the fact that column axial load increased with drift (as predicted in experimental testing design). As explained in [29], the axial load was applied through vertical rods restrained by an already compressed, vertically positioned, linear spring mounted on each column. The spring length and stiffness were designed such that further compression of it due to lateral drift marginally increased the axial load, for example maximum of further 2 mm compression compared to initial 20 mm compression (please refer [29] for full explanation). Whilst this increase was deemed insignificant in low range of displacement, it becomes significant when lateral drift becomes substantial. Therefore, the modelling predictions in long range of drift are unreliable, however this drift range is rarely of any practical significance.

For a quantitative comparison, a peak force prediction error is defined as Eq. (3) and the results listed in Table 9.
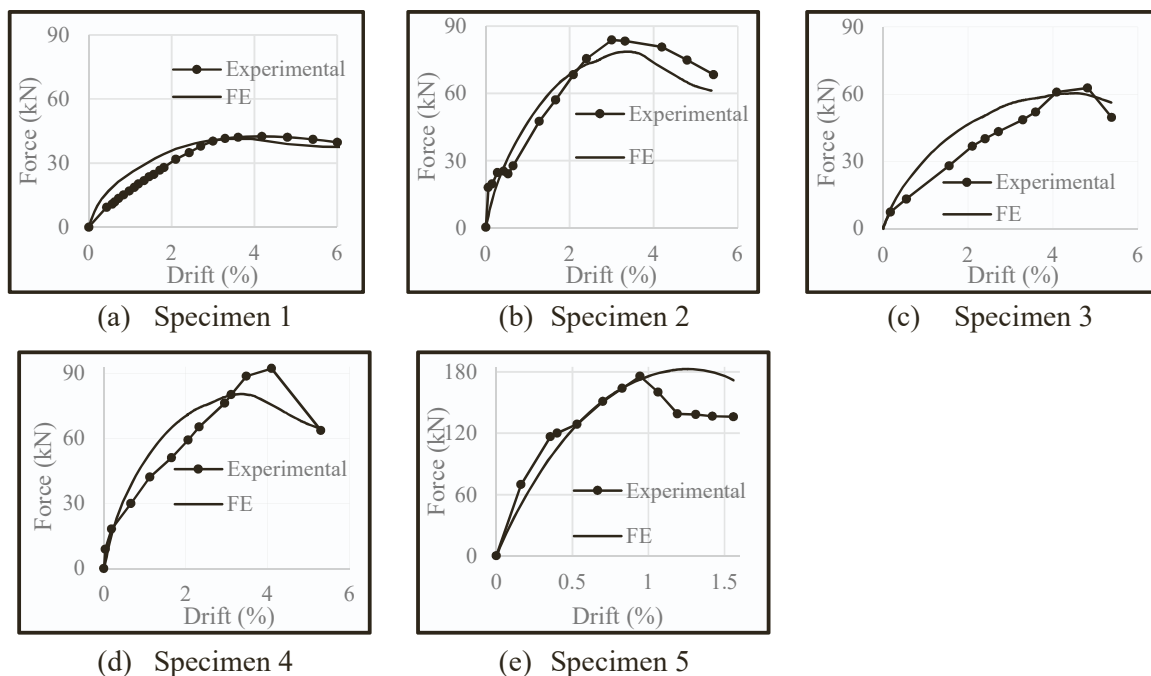
$$\frac{(V_{\max})_{FE} - (V_{\max})_{EXP}}{(V_{\max})_{EXP}} \tag{3}$$

where EXP and FE refer to the experimental and finite element results respectively. The error ranged from −12.1% to +3.5% signifying the good capability of the model to predict the peak experimental strength, with mostly conservatism. In addition, the relative sliding between the top of the 1st course and the bottom of the 8th course was measured and compared against the experimental observation which showed that the models adequately captured the sliding of the masonry units as shown in Table 9.

The best match of the experimental results for ungrouted specimens (2, 3 and 4) shown in Fig. 12 was obtained when interface stiffness coefficients in the global X direction were calibrated to 0.15 MPa/mm (K_{nn}) and 0.11 MPa/mm (K_{ss}) for the column-masonry infill and bed joint interfaces respectively (see Table 7). These stiffness coefficients corresponded to the sliding direction of the masonry infill and about 36% greater coefficients for column-masonry infill indicates that the presence of dry bed joints resulted in the joints being more flexible. In comparison to the values for traditional MIFs (Table 1), the stiffness coefficients are significantly lower which is also true for the coefficients in the global Y direction with K_{tt} = 0.04 MPa/mm and K_{nn} = 0.85 MPa/mm for column-masonry infill and bed joint interfaces respectively. An artificially high stiffness coefficient in the global Z direction were used in the calibration process (K_{ss}=1.0 MPa/mm for column-masonry infill

Table 9
FE results.

Specimen	$V_{\max}$ (kN)	Error in $V_{\max}$ (FE-Exp)/ Exp* 100 (%)	Relative sliding (mm)	Error in relative sliding (FE-Exp)/ Exp* 100 (%)
1	41.3	-2.9%		
2	78.6	-4.5%	69.2	+8.1%
3	60.5	-2.7%	67.6	-17.6%
4	80.4	-12.1%	67.9	-11.4%
5	182.7	+3.5%	19.9	-5.2%

(a) Specimen 1

(b) Specimen 2

(c) Specimen 3

(d) Specimen 4

(e) Specimen 5

Fig. 12. Force-drift relationship of specimens.

and K_{tt}=10.0 MPa/mm for bed joint interfaces) to represent the presence of interlocking mechanisms (T&G and lugs) that prohibited the out-of-plane movement of the masonry infill.

For grouted specimen (5), the column-masonry infill properties remained unchanged from that of the ungrouted specimens because the vertical alignment mortar was present in both types of specimens. However, the bed joint properties required alteration in the calibration process to include the grouting effect that resulted in about 18% and 670% increase in K_{nn} and K_{ss} respectively compared to that of the ungrouted specimens. The presence of beam and relatively undamaged horizontal mortar between the beam and the masonry infill at top led to only marginal increase in K_{nn}. Contrarily, the grout contributed much higher in the sliding direction (K_{ss}) due to the vertical mortar joints undergoing extensive damage which created a gap between the masonry infill and the column as shown in Fig. 1. Similar to ungrouted specimens, a relatively higher stiffness coefficient was used in the out-of-plane direction. It is highlighted that stiffness coefficients in the grouted specimen are still considerably smaller than that reported for traditional MIFs which can be attributed to low grout strength use in filling the cores.

5. Sensitivity analyses

5.1. Effects of $f_{ct.f}$ and K_{ss}

The lateral response of SIM-infilled frames is dependent on many factors including aspect ratio, axial load, and the composite material relative strength. Parameteric studies such as that conducted in [25] would inform design. For the scope of this study it was considered appropriate to limit the parametric studies to two areas, influence of the grout strength as one of the objectives of this research and influence of modelling parameter, K_{ss}, which represents joint in-plane stiffness. Further parametric studies are reserved for more advanced modelling that follows in future studies. Such models would alleviate limitations encountered in this research including the lack of strength/stiffness deterioration modelling and head-joint restraint which prevented flexural-dominated response modelling.

The sensitivity of lateral strength and initial stiffness of Specimen 5 to $f_{ct.f}$ was studied through a Monte Carlo simulation using MATLAB. For this purpose, 30 samples of input $f_{ct.f}$ that matched a lognormal distribution with average value of 0.53 MPa and a standard deviation of 0.30 MPa were generated. The resulting data had a range of [0.31 MPa to 0.94 MPa] which were used as input in the numerical model of Specimen 5. The same procedure of Monte Carlo simulation was repeated to study the effect of bed joint Mode II stiffness coefficient (K_{ss}) on the response of the reference specimen (Specimen 2). The reason for choosing this coefficient was that it corresponded to the direction of masonry unit sliding which was one of the significant observations in the experimental testings of SIM-infilled frames as discussed in the Introduction. In this simulation, the input data included average K_{ss} of 0.11 MPa/mm (see Table 7) with 0.30 MPa/mm standard deviation that produced the data range of [0.060 MPa/mm to 0.19 MPa/mm]. The resultant strength and stiffness of the specimens along with the statistical data from the sensitivity analyses are shown in Table 10.

As shown in Table 10, the average strength and stiffness from the sensitivity analysis of $f_{ct.f}$ were 186.0 kN and 16.5 kN/mm, while for K_{ss}, the average strength and stiffness were 78.4 kN and 3.2 kN/mm. The standard deviations of the strength and stiffness of the specimens varied between 0.04 and 0.08. These values show that when rest of the parameters had remained unchanged, a 30% variation in $f_{ct.f}$ resulted in the MIF's strength and stiffness change between 4% and 8%. Therefore, it can be concluded that both $f_{ct.f}$ and K_{ss} have marginal effects on the behaviour of SIM-infilled frames. The sensitivity analyses of other interface properties are identified as recommendations for future investigations. In addition, the model can be improved by incorporating flexible perpends instead of rigid joints to enable modelling of MIFs with different aspect ratios.

6. Summary and conclusions

The objective of the present paper was to develop, validate and apply FE models to study the lateral load response of MIFs with SIM. Two sensitivity analyses were conducted one aimed at testing modelling sensitiveness (to a stiffness coefficient) and the other aimed at investigating variance in response due to a change in a physical property (grout tensile strength). The research novelty included incorporating sliding of masonry units that were observed during the experimental investigations of 4 MIF specimens.

Cohesive traction-separation interface elements were used to simulate the large experimental deformations observed in the column-masonry infill and bed joint interfaces. The other interfaces that included beam-masonry infill and the perpends were rigidly connected due to lesser degree of damage sustained in the experiment. This constraint in the modelling is unsuitable for flexural-dominated structures, i.e. high aspect (height-to-width) ratio infills. Both concrete and masonry materials were simulated using CDP. The reinforcing bars were modelled as elastic-perfectly plastic behaviour that assumed perfect bond development with the surrounding concrete material.

A large number of analyses was carried out using numerous interface properties of traction-separation model through the calibration process. The best match of the experimental results for ungrouted specimens was achieved when stiffness coefficients in the global X or sliding direction were calibrated to 0.15 MPa/mm (K_{nn}) and 0.11 MPa/mm (K_{ss}) for the column-masonry infill and bed joint interfaces respectively (see Table 7). A 36% higher coefficient for column-masonry infill was attributed to the presence of dry bed joints that resulted in flexible joints. The coefficients were observed to be significantly lower than that reported for traditional MIFs (Table 1) which were also found to be true for the tangential (global Y and Z) directions. The presence of grouted cores in Specimen 5 resulted in approximately 18% and 670% increase in K_{nn} and K_{ss} respectively compared to that of the ungrouted specimens where K_{ss} corresponded to the sliding direction. The grout contributed much higher in the sliding direction (K_{ss}) due to the vertical mortar joints undergoing extensive damage which created a gap between the masonry infill and the column as shown in Fig. 1.

The sensitivity analyses of mechanical properties of interface were performed using Monte Carlo simulation. The results indicated that the Mode II stiffness coefficient of bed joint and grout tensile strength had marginal influence on the overall behaviour of SIM-infilled frames.

Whilst the knowledge generated in this research will be helpful towards development of SIM-infilled construction method for improved performance in seismic areas, future refined numerical studies would have to include 1) realistic modelling of head-joint interfaces to allow accurate vertical movement and flexural (not just shear) deformation predictions for broader parametric studies that can inform future building designs; 2) inclusions of out-of-plane restraint that corresponds to the definite strength of the directional interlocking features; 3) modelling dynamic response supported by suitable tests and conducting special studies focused on assessing infilled masonry cracking and falling

Table 10
Results of sensitivity analysis.

	Range	Mean	Standard deviation
Effect of change of grout tensile strength, $f_{ct.f}$, on response of Specimen 5			
Strength (kN)	181.4 – 190.7	186.0	0.07
Stiffness (kN/mm)	16.1 – 16.8	16.5	0.05
Effect of change of stiffness coefficient, K_{ss}, on response of Specimen 2			
Strength (kN)	70.2 – 82.2	78.4	0.04
Stiffness (kN/mm)	2.9 – 3.5	3.2	0.08

hazards under earthquake loads; 4) determining limits on the core grout strength that can still promote limited sliding and hence less stiffness interaction with the frame whilst providing adequate insulating properties; and 5) incorporating and modelling features at masonry-frame interface aiming to increase resiliency against out-of-plane failure.

CRediT authorship contribution statement

Sonam Dorji: Conceptualization, Methodology, Investigation, Project administration, Formal analysis, Writing – original draft. **Hossein Derakhshan**: Methodology, Funding acquisition, Resources, Supervision, Data interpretation, and Writing – review & editing. **David P Thambiratnam** and **Alireza Mohyeddin**: Supervision, Writing – review & editing.

Declaration of Competing Interest

The authors declare that there is no conflict of interest.

Acknowledgements

References

[1] Bose S. Analytical and numerical framework for the seismic assessment of infilled RC frames [PhD Thesis]. Unite States: The State University of New York; 2019.

[2] Kaushik H, Rai DC, Jain S. Code approaches to seismic design of masonry-infilled reinforced concrete frames: a state-of-the-art review. Earthq Spectra 2006;22: 961–83.

[3] Khan NA, Monti G, Nuti C, Vailati M. Effects of infills in the seismic performance of an rc factory building in Pakistan. Buildings 2021;11:276.

[4] Kumar M, Rai DC, Jain SK. Ductility reduction factors for masonry-infilled reinforced concrete frames. Earthq Spectra 2015;31:339–65.

[5] Yekrangnia M, Asteris PG. Multi-strut macro-model for masonry infilled frames with openings. J Build Eng 2020;32:101683.

[6] ASCE [American Society of Civil Engineers]. Seismic evaluation and retrofit of existing buildings. ASCE/SEI 41–17 ed. Reston, VA: American Society of Civil Engineers; 2017.

[7] TMS [The Masonry Society]. TMS 402/602 building code requirements and specifications for masonry structures, 2016. Farmington Hills: American Concrete Institute; 2017.

[8] NZSEE [New Zealand Society for Earthquake Engineering]. The seismic assessment of existing buildings. New Zealand: New Zealand Society for Earthquake Engineering; 2017.

[9] Feng Y, Wu X, Zhang S. Failure modes of masonry infill walls and influence on RC frame structure under earthquake. Earthquake Engineering Research Institute; 2014.

[10] Varum H, Furtado A, Rodrigues H, Dias-Oliveira J, Vila-Pouca N, Arêde A. Seismic performance of the infill masonry walls and ambient vibration tests after the Ghorka 2015, Nepal earthquake. Bull Earthq Eng 2016;15:1185–212.

[11] Barbosa AR, Fahnestock LA, Fick DR, Gautam D, Soti R, Wood R, et al. Performance of medium-to-high rise reinforced concrete frame buildings with masonry infill in the 2015 Gorkha, Nepal, earthquake. Earthq Spectra 2017;33:197–218.

[12] Furtado A, Vila-Pouca N, Varum H, Arêde A. Study of the seismic response on the infill masonry walls of a 15-storey reinforced concrete structure in Nepal. Buildings 2019;9:39.

[13] Hyland C, Smith A. CTV building collapse investigation for Department of Building and Housing. Christchurch, New Zealand: [Dept. of Building and Housing]; 2012.

[14] Kam WY, Pampanin S, Elwood K. Seismic performance of reinforced concrete buildings in the 22 February Christchurch (Lyttelton) earthquake. Bull NZ Soc Earthq Eng 2011;44:239–78.

[15] Mosalam KM, Gunay S. Progressive collapse analysis of reinforced concrete frames with unreinforced masonry infill walls considering in-plane/out-of-plane interaction. Earthq Spectra 2015;31:921–43.

[16] Kafle B, Mohyeddin A, Wibowo A. A report on the visit to the region stricken by the Wenchuan earthquake. Electron J Struct Eng 2008. Special Issue:1.

[17] De Angelis A, Pecce MR. The structural identification of the infill walls contribution in the dynamic response of framed buildings. Struct Control Health Monit 2019;26:e20405.

[18] Milanesi RR, Morandi P, Manzini CF, Albanesi L, Magenes G. Out-of-plane response of an innovative masonry infill with sliding joints from shaking table tests. J Earthq Eng 2022;26(4):1789–823. https://doi.org/10.1080/13632469.2020.1739173.

[19] Milanesi RR, Hemmat M, Morandi P, Totoev Y, Rossi A, Magenes G. Modeling strategies of ductile masonry infills for the reduction of the seismic vulnerability of RC frames. Front Built Environ 2020;6. https://doi.org/10.3389/fbuil.2020.601215.

[20] Morandi P, Milanesi RR, Magenes G. Innovative solution for seismic-resistant masonry infills with sliding joints: in-plane experimental performance. Eng Struct 2018;176:719–33. https://doi.org/10.1016/j.engstruct.2018.09.018.

[21] Bikçe M, Emsen E, Erdem MM, Bayrak OF. An investigation on behavior of RC frames with non-interacting infill wall. Eng Struct 2021;245. https://doi.org/10.1016/j.engstruct.2021.112920.

[22] Erdem MM, Emsen E, Bikçe M. Experimental and numerical investigation of new flexible connection elements between infill walls-RC frames. Constr Build Mater 2021;296. https://doi.org/10.1016/j.conbuildmat.2021.123605.

[23] Preti M, Bolis V, Stavridis A. Seismic infill–frame interaction of masonry walls partitioned with horizontal sliding joints: analysis and simplified modelling. J Earthq Eng 2019;23(10):1651–77. https://doi.org/10.1080/13632469.2017.1387195.

[24] Preti M, Neffati M, Bolis V. Earthen masonry infill walls: use of wooden boards as sliding joints for seismic resistance. Constr Build Mater 2018;184:100–10. https://doi.org/10.1016/j.conbuildmat.2018.06.184.

[25] Bolis V, Stavridis A, Preti M. Numerical investigation of the in-plane performance of masonry-infilled RC frames with sliding subpanels. J Struct Eng 2017;143(2): 04016168.

[26] Vailati M, Di Gangi G, Quaranta G. Thermo-mechanical characterization and hysteretic behavior identification of innovative plastic joint for masonry infills in reinforced concrete buildings. J Build Eng 2023;65. https://doi.org/10.1016/j.jobe.2022.105803.

[27] Hossain MA, Totoev YZ, Masia M. Experimental assessment of large displacement cyclic in-plane shear behaviour of semi-interlocking masonry panels. Int J Mason Res Innov 2019;4:378.

[28] Hossain MA, Totoev YZ, Masia MJ. Experimental investigation of frictional behavior of mortarless surface in semi-interlocking masonry under cyclic displacement. J Mater Civ Eng 2020;32(9). https://doi.org/10.1061/(ASCE)MT.1943-5533.0003333.

[29] Dorji S, Derakhshan H, Thambiratnam DP. Experimental investigation of semi-interlocking mortarless masonry-infilled frames. Structures 2022;43:1913–31.

[30] Al-Chaar G, Issa M, Sweeney S. Behavior of masonry-infilled nonductile reinforced concrete frames. J Struct Eng 2002;128.

[31] Basha SH, Kaushik HB. Behavior and failure mechanisms of masonry-infilled RC frames (in low-rise buildings) subject to lateral loading. Eng Struct 2016;111: 233–45.

[32] Mehrabi AB. Behavior of masonry-infilled reinforced concrete frames subjected to lateral loadings [PhD Thesis]. United States: University of Colorado; 1994.

[33] Tekeli H, Aydin A. An experimental study of the seismic behavior of infilled RC frames with opening. Sci Iran Trans A Civ Eng 2017;24:2271–82.

[34] Suzuki T, Choi H, Sanada Y, Nakano Y, Matsukawa K, Paul D, et al. Experimental evaluation of the in-plane behaviour of masonry wall infilled RC frames. Bull Earthq Eng 2017;15:4245–67.

[35] Mohyeddin A, Dorji S, Gad EF, Goldsworthy HM. Inherent limitations and alternative to conventional equivalent strut models for masonry infill-frames. Eng Struct 2017;141:666–75.

[36] Kareem KM, Abdulla KF, Panto B, Cunningham LS. Numerical simulation of the in-plane lateral response of RC infill frames using a FEM-DMEM modelling approach. J Build Eng 2022;51:104305.

[37] Dassault Systemes. Abaqus analysis user's guide. Providence, RI; 2014.

[38] Zuo H, Zhang W, Wang B, Gu X. Force–displacement relationship modelling of masonry infill walls with openings in hinged steel frames. Bull Earthq Eng 2021;20: 349–82.

[39] Pal S, Yadav S, Thakur O, Kashyap R. Study of behavior of the masonry infill structures subjected to lateral loads. Singapore: Springer Singapore; 2022.

[40] Emami SM, Mohammadi M. Influence of vertical load on in-plane behavior of masonry infilled steel frames. Earthq Struct 2016;11:609–27.

[41] Nasiri E, Liu Y. Development of a detailed 3D FE model for analysis of the in-plane behaviour of masonry infilled concrete frames. Eng Struct 2017;143:603–16.

[42] Chandel VS, Yamini, Sreevalli I. Numerical study on influence of masonry infill in an RC frame. Asian J Civ Eng 2018;20:1–8.

[43] Bolhassani M, Hamid AA, Lau ACW, Moon F. Simplified micro modeling of partially grouted masonry assemblages. Constr Build Mater 2015;83:159–73.

[44] Najarkolaie K, Mohammadi M, Fanaie N. Realistic behavior of infilled steel frames in seismic events: experimental and analytical study. Bull Earthq Eng 2017;15: 5365–92.

[45] Zhai C, Kong J, Wang X, Chen Z. Experimental and finite element analytical investigation of seismic behavior of full-scale masonry infilled RC frames. J Earthq Eng 2016;20:1171–98.

[46] Veronese RBA, Medeiros WA, Parsekian GA, Shrive NG. Numerical analysis of eco-friendly ductile cementitious composite influence on structural masonry reinforcement. Eng Struct 2022;252:113686.

[47] Khatiwada A, Jiang H. Numerical modeling of masonry infilled reinforced concrete moment-resisting frame. The thirtienth KKHTCNN symposium on civil engineering. Taiwan; 2017.

[48] Zahra T. Strategies for improving the response of drystack masonry to compression [PhD Thesis]. Australia: Queensland University of Technology; 2017.

[49] Shi T, Zhang X, Hao H, Chen C. Experimental and numerical investigation on the compressive properties of interlocking blocks. Eng Struct 2021;228:111561.

[50] Emami S, Mohammadi M, Lourenço P. Equivalent diagonal strut method for masonry walls in pinned connection and multi-bay steel frames. J Seismol Earthq Eng 2017;19:299.

[51] AM [Adbri Masonry]. Versaloc walling system; 2022. https://www.adbrimasonry. com.au/wp-content/uploads/2021/09/19450-Versaloc-12pp-Brochure-May-2019. pdf. [Accessed 16 Feb, 2022].

[52] Dorji S, Derakhshan H, Thambiratnam DP, Zahra T, Mohyeddin A. Behaviour and material properties of Versaloc semi-interlocking mortarless masonry. Mater Struct 2023;56:17.

[53] Behnam H, Kuang JS, Samali B. Parametric finite element analysis of RC wide beam-column connections. Comput Struct 2018;205:28–44.

[54] Deng H, Sun B. Finite element modeling and mechanical behavior of masonry-infilled RC frame. Open Civ Eng J 2016;10:76–92.

[55] Mark JT, Sreevalli IY. Numerical study on lateral performance of RC frame with strong masonry infill. Asian J Civ Eng 2021;22:551–63.

[56] Abasi A, Hassanli R, Vincent T, Manalo A. Influence of prism geometry on the compressive strength of concrete masonry. Constr Build Mater 2020;264:120182.

[57] Oliveira RLG, Rodrigues JPC, Pereira JM, Lourenço PB, Ulrich Marschall H. Normal and tangential behaviour of dry joints in refractory masonry. Eng Struct 2021;243: 112600.

[58] Wosatko A, Winnicki A, Polak MA, Pamin J. Role of dilatancy angle in plasticity-based models of concrete. Arch Civ Mech Eng 2019;19:1268–83.

[59] Abdulla KF, Cunningham LS, Gillie M. Simulating masonry wall behaviour using a simplified micro-model approach. Eng Struct 2017;151:349–65.

[60] Wang J, Jivkov AP, Li QM, Engelberg DL. Experimental and numerical investigation of mortar and ITZ parameters in meso-scale models of concrete. Theor Appl Fract Mech 2020;109:102722.

[61] ASTM [American Society for Testing and Materials]. C496/C496 – 17 standard test method for splitting tensile strength of cylindrical concrete specimens. West Conshohocken, United States: ASTM International; 2017.

[62] Wu J-R, Di Sarno L, Freddi F, D'Aniello M. Modelling of masonry infills in existing steel moment-resisting frames: nonlinear force-displacement relationship. Eng Struct 2022;267:114699.

[63] Abed F, Oucif C, Awera Y, Mhanna H, Alkhraisha H. FE modeling of concrete beams and columns reinforced with FRP composites. Def Technol 2021;17:1–14.

[64] Fallahi M, Sayyar Roudari S, Haghighifar M, Madandoost R. Modeling of reinforced concrete frames with infill walls under cyclic loading strengthening with CFRP. Am J Eng Appl Sci 2018.

[65] Roudane B, Adanur S, Altunışık AC. Numerical modeling of masonry infilled reinforced concrete building during construction stages using ABAQUS software. Buildings 2019;9:181.

[66] SA [Standards Australia]. Masonry structures. Sydney: New South Wales 2001: SAI Global Limited: Standards Australia; 2018.

[67] Kalkan I. Lateral torsional buckling of rectangular reinforced concrete beams. Acids Struct J 2014;111:71–81.

[68] Maison BF, Speicher MS. Loading protocols for ASCE 41 backbone curves. Earthq Spectra 2016;32(4). https://doi.org/10.1193/010816EQS007EP.

[69] Gatto K, Uang C-M. Effects of loading protocol on the cyclic response of wood-frame shearwalls. J Struct Eng ASCE 2003;129:1384–93.

[70] Panyakapo P. Cyclic pushover analysis procedure to estimate seismic demands for buildings. Eng Struct 2014;66:10–23.